PHYSICAL REVIEW A, VOLUME 63, 043412

Photoionization spectra in parallel electric and magnetic fields

A. S. Johnson and F. Mota-Furtado

Department of Mathematics, Royal Holloway, University of London, Egham, Surrey TW20 0EX, United Kingdom

(Received 2 August 2000; published 19 March 2001)

We present a quantum-mechanical method to evaluate photoionization spectra of atoms in parallel applied electric and magnetic fields, valid for a wide range of energies and field strengths. We identify different symmetry regions in configuration space and use *R*-matrix propagation, a frame transformation and a two-dimensional matching procedure to asymptotically defined solutions to solve the Schrödinger equation over all space. We use quantum defect theory to take into account nonhydrogenic atomic cores. We illustrate the method for the hydrogen atom in laboratory strength fields and for strong fields. We analyze the main features of the photoionization spectra for electric and magnetic-field strengths of 51.4 $\mathrm{k\,V\,cm^{-1}}$ and 470 T, respectively. We identify three types of resonances, defined by their behavior upon varying the external fields and we explain this behavior in terms of the associated wave functions.

DOI: 10.1103/PhysRevA.63.043412 PACS number(s): 32.60.+i, 32.80.Fb

I. INTRODUCTION

The analysis of the spectrum of an atom in a magnetic field has proved very fruitful as it provides an example of an experimentally accessible system whose classical Hamiltonian is chaotic for certain field strengths and energy ranges. Much has been learned about the effects of classical chaos through the semiclassical analysis of such real systems [1]. In addition, new *ab initio* quantum-mechanical techniques have been developed to calculate the photoabsorption and photoionization cross sections for an atom in a magnetic field [2–4].

An atom in a parallel static electric and magnetic field is an example of a nonseparable Hamiltonian system with less symmetry than an atom in a magnetic field alone, due to the asymmetry introduced by the applied electric field. The electric field also changes the asymptotic nature of the potential from a one-dimensional Coulomb potential to a Stark potential, which in general destroys the Coulomblike Rydberg series of bound and resonance states. In fact in many experiments it is difficult to remove small residual stray electric fields so that the combined field problem is of practical significance in addition to its fundamental interest.

In recent years a number of calculations have been performed for atoms in parallel fields, both in the bound state region of the spectrum (see Ref. [5] and references therein) and in the continuum [6,7]. The theoretical methods used to calculate the photoexcitation cross sections follow procedures very similar to the ones used in atoms in a magnetic field only. There also exists some experimental data for bound-state spectra [8].

We present in this paper a fully quantum-mechanical method to calculate the photoionization spectrum of an atom in parallel electric and magnetic fields for a wide range of energies and field strengths. The approach is based on the method developed by O'Mahony and Mota-Furtado for magnetic fields [3] and adapted by Moser [9] to cover a very wide energy range. We use *R*-matrix propagation [10,11] to propagate the solution of the Schrödinger equation in spherical coordinates from a small initial radius to the asymptotic region. We define appropriate asymptotic solutions for parallel fields in cylindrical coordinates and then match them through a two-dimensional matching procedure to the propagated solutions, in order to obtain the solution over all space and hence the photoionization cross section. We illustrate the method for the hydrogen atom and we show how to classify different cases depending on the relative strength of the applied electric and magnetic fields. We consider the case of both strong fields and of laboratory strength fields. We examine the effect of changing the electric and magnetic fields on the positions of the resonances and we identify different types of resonances from plots of their associated wave functions.

The paper is structured as follows. In Sec. II we show how we partition configuration space depending on the strength of the potentials acting on the ionizing electron and how we propagate the solution to the asymptotic region. We explain in Sec. III, through the study of a one-dimensional model, how to to generate analytic asymptotic solutions for the problem. In Sec. IV we show how adiabatic curves can be used to give physical insight and to make the numerical work more efficient. In Secs. V and VI we discuss the matching procedure, the evaluation of the cross section and the use of the complex coordinate rotation method to examine the resonance wave functions. Atomic units will be used throughout unless otherwise stated.

II. PARTITION OF COORDINATE SPACE

The most obvious effect in imposing external parallel fields is the definition of a preferential direction in space, the direction of the parallel applied fields. This breaks the rotational symmetry of the atom. The nonrelativistic Hamiltonian operator for a hydrogen atom in parallel fields directed along the z axis can be written, using spherical polar coordinates (r,θ,ϕ), as

$$H=-\frac{1}{2}\nabla^2-\frac{1}{r}+\beta L_z+\frac{1}{2}\beta^2 r^2\sin^2\theta-fr\cos\theta, \quad (1)$$

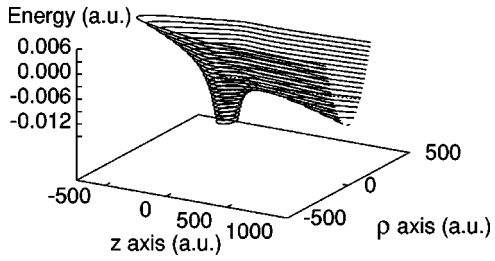

FIG. 1. Lines of constant potential for an atom in parallel electric and magnetic fields of strengths 51.4 kV cm^{-1} (1×10^{-5} a.u.) and 470 T (1×10^{-3} a.u.), respectively. The dotted line represents the Stark saddle energy that corresponds to the classical ionization threshold for zero magnetic field. The lines have been reflected through $\rho=0$ to give a clearer picture. The graph shows the presence of a harmonic oscillator in ρ produced by the quadratic Zeeman term and the breaking of the symmetry in z by the electric field.

where we take the proton mass to be infinite. $\beta=B/B_c$ ($B_c=4.7\times10^5\ T$) and $f=F/F_c$ ($F_c=5.14\times10^9$ V cm^{-1}) represent the magnetic- and electric-field strengths, respectively, in atomic units, and L_z is the z component of the angular momentum. The externally applied potential is represented by the terms,

$$V_{ext}=\frac{1}{2}\beta^2 r^2\sin^2\theta-fr\cos\theta, \tag{2}$$

apart from the linear Zeeman term, and is independent of the azimuthal angle ϕ. Hence, in this alignment of fields, the full Hamiltonian is also independent of ϕ and the magnetic quantum number m is a good quantum number. L_z is a conserved quantity and only contributes to the uniform energy shift of magnitude βm. Equation (1) can also be expressed using cylindrical polar coordinates (ρ,ϕ,z), as

$$H=-\frac{1}{2}\nabla^2-\frac{1}{\sqrt{\rho^2+z^2}}+\beta L_z+\frac{1}{2}\beta^2\rho^2-fz, \tag{3}$$

showing that the Hamiltonian does not exhibit reflection symmetry about the $z=0$ plane. This is a major difference to the magnetic field case as now we have to deal with different asymptotic behavior depending on the two possible limits in the directions $z\to+\infty$ and $z\to-\infty$. Ionization is physically restricted to the positive z direction of space as illustrated by the diagram of the lines of constant potential for an atom in parallel electric and magnetic fields, in Fig. 1.

Equation (2) can be used to show the relative importance of the applied fields. For fields typically of laboratory strength, i.e., $f\approx10^{-6};\beta\approx10^{-5}$, in the region contained inside of a sphere of a radius of the order of 10 a.u., the Coulomb field is of order $1/r\approx10^{-1}$ a.u. $\gg V_{ext}$. Therefore, in this region, the problem has spherical symmetry as the Coulomb field is dominant and the applied fields act as small perturbations. One can thus identify a spherical region that contains the ground state and the low excited states, which are unaffected by the applied fields. For larger radii the Coulomb potential and the external fields are comparable and affect strongly the Rydberg states or states excited to the continuum. There is then a competition between the fields, which is reflected in a competition between the spherical-cylindrical nature of the potentials and is directly responsible for the onset of chaos in the system's classical counterpart. An asymptotic region can be identified when the ionizing electron is mainly affected by the applied fields, which are several orders of magnitude greater then the Coulomb field felt at that distance.

We can then describe in general the motion of an electron in a hydrogen atom excited to a continuum state (or indeed to a Rydberg state) by dividing space into three different regions. The boundaries between these regions will depend on the magnitude of the external fields. The radial ranges indicated below are for laboratory strength fields and will assume different values for stronger fields. They are as follows:

(i) an internal region where the Coulomb field dominates, for $r\leqslant a=100$ a.u.;

(ii) a strong-mixing region where all the fields are equally important and have to be treated on an equal footing, for $a=100$ a.u. $\leqslant r\leqslant b=1000$ a.u.;

(iii) an asymptotic region where the external fields dominate, for $r\geqslant b=1000$ a.u.

We will solve the Schrödinger equation in each of these regions separately using an appropriate procedure and then find the solution over all space by enforcing continuity of the solutions and their derivatives at their common boundaries. The motion of the electron in the first region can be described as in the field-free case, in terms of regular Coulomb functions. An important task consists then of describing the motion of the electron in region (ii) where the problem is nonseparable. Region (iii) is chosen so that we can define an accurate asymptotic solution. Nonhydrogenic atoms are considered by subdividing region (i) in order to take into account the multielectron atomic core region.

A. The internal region

1. Hydrogen atom

In this region the Coulomb term $-1/r$ is dominant and the effect of the external fields is negligible. Hence we consider the region to be spherical and to extend up to a radial distance $r=a$, for which the applied fields can still be neglected; we use spherical coordinates (r,θ,ϕ) within the region, so that the Schrödinger equation associated with Hamiltonian (1) becomes separable. We solve it by decomposition in partial waves, according to the orbital angular momentum quantum number l and we write the lth partial wave at an energy ε, $\psi_{\varepsilon l}(\underline{r})$, as

$$\psi_{\varepsilon l}(\underline{r})=\frac{s_{\varepsilon l}(r)}{r}Y_{lm}(\theta,\phi), \tag{4}$$

where $s_{\varepsilon l}$ is the regular Coulomb function [12] evaluated at energy ε and Y_{lm} are the spherical harmonics.

The total wave function $\Psi_{\varepsilon}(\underline{r})$, at an energy ε, can then in general be written as

$$\Psi_{\varepsilon}(\underline{r}) = \sum_{l} A_{\varepsilon l}\psi_{\varepsilon l}(\underline{r}), \tag{5}$$

where the $A_{\varepsilon l}$'s are constants to be determined later when the solutions are matched across their common boundaries. As our method uses the R matrix, i.e., the inverse of the logarithmic derivative of the solution, knowledge of the solution (4), and its derivative in this region, determines the R matrix at the boundary $r=a$, $\mathbf{R}(a)$, namely,

$$R_{ll'}(a) = s_{\varepsilon l}(a)[s'_{\varepsilon l}(a)]^{-1}\delta_{ll'}. \tag{6}$$

2. Nonhydrogenic atoms

For nonhydrogenic atoms the internal region needs to be divided into two subregions:

(i) subregion (I a)—an inner multielectron region where the ionizing electron interacts with all the other electrons and the nucleus of the atom;

(ii) subregion (I b)—a Coulomb region where the ionizing electron moves under the influence of the Coulomb field alone as the external fields are negligible.

Typically the value of the boundary radius between these two regions is of about 10 a.u., so that the inner subregion contains the atomic core of the atom. The ionizing electron is initially excited in this region and interacts with the other particles in the core. Once it goes to subregion (I b), it is outside the core and moves in the Coulomb field of the ion; then the lth partial solution of the Schrödinger equation is written as

$$\psi_{\varepsilon l}(\underline{r}) = \left(\frac{s_{\varepsilon l}(r) + c_{\varepsilon l}(r)\tan \pi\mu_l}{r}\right) Y_{lm}(\theta,\phi), \tag{7}$$

where $c_{\varepsilon l}$ is the irregular Coulomb function evaluated at energy ε, and μ_l are the field free quantum defects, which represent the effect of the core on the excited electron's wave function [12]. Quantum defects can be either calculated *ab initio* or obtained from experimental energy levels. Usually $\mu_l = 0$ for $l>4$, as the atomic centrifugal barrier keeps higher angular momentum states outside of the core region. The total wave function $\Psi_{\varepsilon}(r)$, can be evaluated at any r in the range 10 a.u.$\leqslant r \leqslant a = 100$ a.u. by the use of Eq. (5), with the lth partial wave $\psi_{\varepsilon l}(\underline{r})$ given by expression (7).

The method we present here remains the same as for hydrogen, once the wave function in the internal region is defined as above, leading to a different R matrix at the boundary $r=a$, which includes the effect of the quantum defects, namely,

$$R_{ll'}(a) = [s_{\varepsilon l}(a) + c_{\varepsilon l}(a)\tan \pi\mu_l] \times [s'_{\varepsilon l}(a) + c'_{\varepsilon l}(a)\tan \pi\mu_l]^{-1}\delta_{ll'}. \tag{8}$$

B. The strong-mixing region

In this region the competition between the spherically symmetric Coulomb potential and the cylindrical symmetry of the diamagnetic potential renders the Hamiltonian nonseparable. The region extends from a radius $r=a$ to a large radius $r=b$ and as no approximations can be made, the full Hamiltonian must be considered. The radius $r=b$ is chosen large enough so that the solutions obtained for the Schrödinger equation for $r>b$ are the asymptotic solutions, which will be expressed in cylindrical coordinates.

We will solve the Schrödinger equation in the region $[a,b]$ by using the R-matrix method. We diagonalize the full Hamiltonian in Eq. (1) plus the Bloch operator L given by

$$L = \frac{1}{2}\left[\delta(r-b)\frac{d}{dr} - \delta(r-a)\frac{d}{dr}\right]\delta_{ij} \tag{9}$$

in a basis set of shifted Legendre polynomials $g_n(r)$ and spherical harmonics $Y_{lm}(\theta,\phi)$, over region $[a,b]$. The Bloch operator [13] ensures the Hermiticity of $H+L$ in the finite region $[a,b]$. The shifted Legendre polynomials, $\{g_n(r)\}$, defined by

$$g_n(r) = \sqrt{\frac{2n-1}{b-a}}P_{n-1}\left[\frac{2}{b-a}\left(r - \frac{b+a}{2}\right)\right], \tag{10}$$

where P_n is a Legendre polynomial of degree n, form an orthonormal basis set over the region [10]. All of the matrix elements of $H+L$ can be calculated analytically in this basis. Assuming this diagonalization yields eigenvectors c^k_{nl} and eigenvalues ε_k, we can express the R matrix at $r=b$, $\mathbf{R}(b)$, in terms of the R matrix at $r=a$, $\mathbf{R}(a)$, as follows (see Baluja *et al.* [10] for further details). Rearranging the Schrödinger equation in the form

$$(H+L-\varepsilon)\Psi_{\varepsilon} = L\Psi_{\varepsilon}, \tag{11}$$

and using the fact that the eigenvalues ε_k and eigenfunctions ψ_k from the diagonalization are such that

$$(H+L)|\psi_k\rangle = \varepsilon_k|\psi_k\rangle \tag{12}$$

then we can write $|\Psi_{\varepsilon}\rangle$ as

$$|\Psi_{\varepsilon}\rangle = \sum_{k,k'} |\psi_k\rangle\langle\psi_k|(H+L-\varepsilon)^{-1}|\psi_{k'}\rangle\langle\psi_{k'}|L|\Psi_{\varepsilon}\rangle \tag{13}$$

or

$$|\Psi_{\varepsilon}\rangle = \sum_{k} \frac{|\psi_k\rangle\langle\psi_k|L|\Psi_{\varepsilon}\rangle}{\varepsilon_k - \varepsilon}. \tag{14}$$

The full wave function Ψ_{ε} can be expressed in a general way as the sum of the product of the lth radial function $U_l(r)$ and the spherical harmonic $Y_{lm}(\theta,\phi)$, as

$$|\Psi_{\varepsilon}\rangle = \sum_{l} \frac{U_l(r)}{r} Y_{lm}(\theta,\phi), \tag{15}$$

The kth eigenfunctions from the diagonalization of $H+L$ are given similarly by

$$|\psi_k\rangle = \sum_{l} \frac{U_{lk}(r)}{r} Y_{lm}(\theta,\phi), \tag{16}$$

with

$$U_{lk}(r)=\sum_n c_{nl}^k g_n(r), \tag{17}$$

where $g_n(r)$ are shifted Legendre polynomials.

Using this notation directly in Eq. (14), we get

$$\sum_l U_l(r)Y_{lm}(\theta,\phi) = \sum_k \sum_l \frac{U_{lk}(r)}{\varepsilon_k-\varepsilon}\frac{Y_{lm}(\theta,\phi)}{2} \times \sum_{l'}\left(U_{l'k}(b)\left.\frac{dU_{l'}}{dr}\right|_{r=b} - U_{l'k}(a)\left.\frac{dU_{l'}}{dr}\right|_{r=a}\right). \tag{18}$$

Projecting out the angular functions by integrating over θ and ϕ, and evaluating the expression at radii $r=a$ and $r=b$, respectively, we get

$$\vec{U}(a)=\mathbf{r}_2\left.\frac{d\vec{U}}{dr}\right|_{r=b} - \mathbf{r}_1\left.\frac{d\vec{U}}{dr}\right|_{r=a}, \tag{19}$$

and

$$\vec{U}(b)=\mathbf{r}_4\left.\frac{d\vec{U}}{dr}\right|_{r=b} - \mathbf{r}_3\left.\frac{d\vec{U}}{dr}\right|_{r=a}, \tag{20}$$

where the four matrices $\mathbf{r}_1$ to $\mathbf{r}_4$, are defined as

$$\mathbf{r}_1=\frac{1}{2}\sum_k \frac{U_{lk}(a)U_{l'k}(a)}{\varepsilon_k-\epsilon}, \quad \mathbf{r}_2=\frac{1}{2}\sum_k \frac{U_{lk}(a)U_{l'k}(b)}{\varepsilon_k-\epsilon},$$
$$\mathbf{r}_3=\frac{1}{2}\sum_k \frac{U_{lk}(b)U_{l'k}(a)}{\varepsilon_k-\epsilon}, \quad \mathbf{r}_4=\frac{1}{2}\sum_k \frac{U_{lk}(b)U_{l'k}(b)}{\varepsilon_k-\epsilon}. \tag{21}$$

Using the formal definition of the R matrix at a radius $r=a$,

$$\vec{U}(a)=\mathbf{R}(a)\left.\frac{d\vec{U}}{dr}\right|_{r=a} \tag{22}$$

and similarly for $\mathbf{R}(b)$, one obtains the following relation between the R matrix at $r=a$ and the R matrix at $r=b$

$$\mathbf{R}(b)=\mathbf{r}_4-\mathbf{r}_3[\mathbf{r}_1+\mathbf{R}(a)]^{-1}\mathbf{r}_2 \tag{23}$$

from Eqs. (19) and (20).

Depending on the field strengths the region $[a,b]$ may be quite large. When the region is large, direct application of Eq. (23) may involve the diagonalization of very large matrices since our basis set would have to span the entire distance $[a,b]$. To minimize the size of the matrices and to reduce program running time, we may subdivide the range $[a,b]$ into smaller sectors and propagate the R matrix through these sectors, using the above procedure recursively (see Stechel *et al.* [11]). Using this method we carry out a diagonalization in each of the smaller sectors and construct local sector matrices $\mathbf{r}_1$ to $\mathbf{r}_4$ as above. We can derive analogous expressions to Eqs. (19) and (20) for the whole region with the four matrices $\mathbf{r}_1$ to $\mathbf{r}_4$, replaced by the so-called global sector R matrices that is the four matrices $\mathbf{R}_1$ to $\mathbf{R}_4$. The global sector R matrices are built up iteratively from the matrices $\mathbf{r}_1$ to $\mathbf{r}_4$ during the propagation of the solution over the whole region. We finally end up with a relationship of the form (23) between $\mathbf{R}(a)$ and $\mathbf{R}(b)$, where $\mathbf{r}_1$ to $\mathbf{r}_4$ are replaced by the global sector matrices, $\mathbf{R}_1$ to $\mathbf{R}_4$. We can thus calculate the R matrix $\mathbf{R}(b)$ at the asymptotic radius $r=b$. To determine the solution over all space we need to match to the asymptotic solutions at $r=b$.

C. The asymptotic region

The asymptotic region is reached when the ionizing electron is moving in a region where the applied fields dominate and the problem becomes separable again. Considering Hamiltonian (3) written in cylindrical coordinates (ρ,ϕ,z), the potential assumes the form

$$V(\underline{r})=-\frac{1}{\sqrt{\rho^2+z^2}}+\frac{1}{2}\beta^2\rho^2-fz. \tag{24}$$

In the limit of large values of z, i.e., $z\to\infty$, the Schrödinger equation associated to Hamiltonian (3) becomes separable in these coordinates, since

$$V(\underline{r})\approx-\frac{1}{|z|}+\frac{1}{2}\beta^2\rho^2-fz+O\left(\frac{1}{|z|^3}\right). \tag{25}$$

The motion in ρ is bounded due to the presence of the magnetic field, as shown in Fig. 1. Accordingly, we choose the asymptotic region to be cylindrical with $c\leqslant z<\infty$ and $0\leqslant\rho<\infty$, taking the boundary $z=c$ to be large enough that the potential can be approximated by its separable limit in Eq. (25). Also we choose $c<b$, so that there is an overlap between this region and the strong-mixing region. When solving the Schrödinger equation associated with the asymptotic Hamiltonian

$$H=-\frac{1}{2}\boldsymbol{\nabla}^2-\frac{1}{|z|}+\frac{1}{2}\beta^2\rho^2-fz, \tag{26}$$

the solution of the equation corresponding to the motion in ρ leads to the so-called Landau states $\Phi_i(\rho,\phi)$, which are the eigenfunctions of a two-dimensional harmonic oscillator. The eigenenergies are represented by E_i [$E_i=\beta(2i+1)$ with $(i=0,1,\ldots)$, for $m=0$]. A full solution at an energy $\boldsymbol{\epsilon}$ can then be expressed in terms of the following analytic expression, for the jth linearly independent solution, as

$$\Psi_{\epsilon j}=\sum_i \Phi_i(\rho,\phi)[S_i(z)\delta_{ij}+C_i(z)K_{ij}], \tag{27}$$

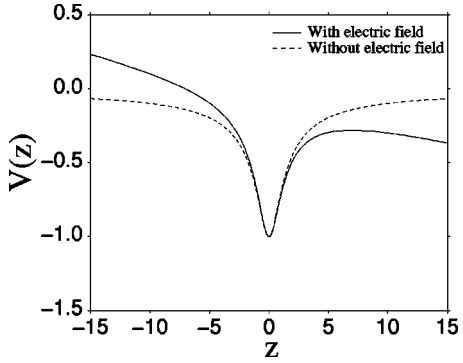

FIG. 2. A plot of the quasi-Coulombic potential in the presence of an electric field of strength 2×10^{-2} a.u. (solid line) compared to the field-free potential (dashed line).

where S_i, C_i are diagonal matrices and K_{ij} is the reactance matrix, or K matrix. $S_i(z)$ and $C_i(z)$ are two linearly independent solutions of the Schrödinger equation associated with the asymptotic Hamiltonian in z,

$$H_z=-\frac{1}{2}\frac{\partial^2}{\partial z^2}-\frac{1}{|z|}-fz, \tag{28}$$

with the corresponding energy $\varepsilon_i=\varepsilon-E_i$. The form of these solutions and their behavior is of central importance for the problem as it will allow us to calculate the K matrix by matching the solutions in the strong-mixing region to those in the asymptotic region, on the arc $r=b$. To get a better understanding of the solutions of Eq. (28) and the resonances they could give rise to, we have used a one-dimensional model system that has the same asymptotic form as Eq. (28) but doesn't have a singularity at $z=0$.

III. A ONE-DIMENSIONAL MODEL SYSTEM

We define a one-dimensional model system in the presence of an applied electric field with Hamiltonian operator given by

$$H=-\frac{1}{2}\frac{d^2}{dz^2}-\frac{1}{\sqrt{1+z^2}}-fz. \tag{29}$$

Such a model was previously used by Su and Eberly [14] in the field free case and in intense laser fields. The potential, given by

$$V=-\frac{1}{\sqrt{1+z^2}}-fz, \tag{30}$$

shows a system that is subjected to a binding potential of Coulomb type but where the singularity at origin is avoided (Fig. 2). For large values of the coordinate z, this model system behaves as a normal Coulomb potential in the presence of an electric-field potential $-fz$, since

$$\frac{1}{\sqrt{1+z^2}}=\frac{1}{|z|}+\frac{1}{2|z|^3}+\cdots=\frac{1}{|z|}+O\left(\frac{1}{|z|^3}\right). \tag{31}$$

To leading order the asymptotic Hamiltonian can then be written as

$$H=-\frac{1}{2}\frac{d^2}{dz^2}-\frac{1}{|z|}-fz, \tag{32}$$

which is precisely the same as the asymptotic Hamiltonian in the coordinate z for the full problem of an atom in parallel electric and magnetic fields, given by Eq. (28).

Two asymptotic limits are to be considered depending on z. $z\to-\infty$, where the excited electron is bound by the Stark potential barrier and $z\to+\infty$, where the excited electron is free to move and ionizes under the influence of the two competing fields, the Coulomb and the electrical field. Asymptotically, if we could neglect completely the Coulombic term in the Hamiltonian of Eq. (32), we would obtain a Schrödinger equation that can be solved analytically. For $z>0$, the solution is an oscillatory Airy function, while for $z<0$ the solution is given by the exponentially decreasing Airy function. However the $1/r$ nature of the Coulombic term influences the solution even at very large distances [15,16] and hence its effect must be included in the definition of the asymptotic solutions if we are to match solutions at reasonable sized radii.

A. Choice of asymptotic solutions

A straightforward procedure to obtain accurate asymptotic solutions is by numerically integrating the Schrödinger equation corresponding to Hamiltonian (32) from a very large distance where the analytic form is known.

If however we want to use analytic asymptotic solutions for this system, we have to find accurate asymptotic solutions for the differential equation,

$$\frac{d^2\chi}{dz^2}+\gamma^2(z)\chi(z)=0, \tag{33}$$

with $\gamma(z)$ given by

$$\gamma^2(z)=2\left(fz+\sqrt{\frac{1}{1+z^2}}+\varepsilon_i\right), \tag{34}$$

where ε_i represents the energy of the system. Possible methods of solution include the use of iterated WKB approximations as used by Seaton for Coulomb functions [17] or of the so-called modified Airy functions (MAF) [18]. These functions are obtained from Airy functions by incorporating terms into the argument of the functions, which mimic the Coulomb behavior for large z. Both of these methods were investigated and checked against one another. We have chosen to use the MAF solutions in what follows. The linearly independent solutions of Eq. (33) can be written as

$$S_{\varepsilon_i}(\xi(z))=\frac{\mathrm{Ai}(\xi(z))}{\sqrt{\xi'(z)}}\quad\text{and}\quad C_{\varepsilon_i}(\xi(z))=\frac{\mathrm{Bi}(\xi(z))}{\sqrt{\xi'(z)}}, \tag{35}$$

where Ai and Bi are the regular and irregular Airy functions and where the argument $\xi(z)$ is given by

$$\xi(z)=\left\{\frac{3}{2}\int_{z_0}^{z}\sqrt{-\gamma^2(z')}dz'\right\}^{2/3} \quad \text{when} \quad \gamma^2(z)<0, \tag{36}$$

$$\xi(z)=-\left\{\frac{3}{2}\int_{z}^{z_0}\sqrt{+\gamma^2(z')}dz'\right\}^{2/3} \quad \text{when} \quad \gamma^2(z)>0. \tag{37}$$

If we refer to a turning point $z=z_0$ of the potential, the case $\gamma^2(z)<0$ corresponds to $z>z_0$, and the case $\gamma^2(z)>0$ corresponds to $z<z_0$, i.e., motion under the barrier.

The MAF solutions are valid if

$$\left|\frac{1}{(\xi')^3}\left(\frac{3(\xi'')^2}{4\xi'}-\frac{\xi'''}{2}\right)\right| \ll |\xi|. \tag{38}$$

Given that, for large z, $\gamma^2(z)$ in Eq. (34) varies approximately linearly with z, the resultant higher-order differentials of $\xi(z)$ in Eq. (38) will be very small in comparison to $\xi(z)$ and the criterion (38) will be met. MAF solutions are finite for all z, avoiding problems of divergence in the vicinity of classical turning points $\gamma^2(z)=0$, common to the WKB approximation. This is an important point when addressing the full problem of an atom in parallel electric and magnetic fields where the solutions may need to be evaluated near classical turning points. The final solution is then given by a linear combination of the two asymptotic solutions in Eq. (35), as

$$\chi(z)=C_1\frac{\mathrm{Ai}(\xi(z))}{\sqrt{\xi'(z)}}+C_2\frac{\mathrm{Bi}(\xi(z))}{\sqrt{\xi'(z)}}, \tag{39}$$

where C_1 and C_2 are constants.

B. Photoexcitation of the one-dimensional system

To check our asymptotic analysis and to get insight into the resonances induced by the asymptotic potential, we solved the one-dimensional system for the Hamiltonian in Eq. (29) by applying the R matrix method over a region $[-a,b]$ and matching to the asymptotic MAF solutions. For the case of an atom in an electric field, the Hamiltonian in Eq. (29) is no longer symmetric with respect to the plane $z=0$ and the corresponding Schrödinger equation can only be characterized by the total energy. In order to determine the solution over all space, at a particular energy ε_i, referred to by $\Psi_{\varepsilon_i}(z)$, we expand the solution in the internal region in terms of a basis set $\{\psi_k(z)\}$, following

$$\Psi_{\varepsilon_i}(z)=\sum_k A_{\varepsilon_i,k}\psi_k(z), \tag{40}$$

where the $A_{\varepsilon_i,k}$'s are a set of energy-dependent coefficients to be determined. The $\{\psi_k(z)\}$ are given by diagonalizing the operator $(H+L)$. We use a basis set of orthonormal shifted Legendre polynomials, $\{g_i(z)\}$, as before where

$$g_i(z)=\sqrt{\frac{2i-1}{b-a}}P_{i-1}\left(\frac{2}{b-a}\left(z-\frac{b+a}{2}\right)\right), \tag{41}$$

where $P_i(z)$ is a Legendre polynomial of degree i. Within this particular basis set, the majority of matrix elements encountered can be evaluated analytically. The diagonalization gives eigenvalues ε_k and eigenvectors C_j^k, which satisfy the equation

$$(H+L)\psi_k(z)=\varepsilon_k\psi_k(z), \tag{42}$$

with $\psi_k(z)$ given by

$$\psi_k(z)=\sum_j C_j^k g_j(z). \tag{43}$$

In our one-dimensional problem we consider the internal region limited by two values of z given by $-a$ and b, where $a,b>0$; $z=-a$ is selected so as to be under the potential barrier on the $(-z)$ side and the value of $z=b$ is chosen to be large enough to meet the accuracy criterion (38) imposed on the definition of the solutions, $S_{\varepsilon_i}(\xi(z))$ and $C_{\varepsilon_i}(\xi(z))$, according to Eq. (35). Since $z=-a$ was chosen to be in the classically forbidden region, the asymptotic solution is then given by the exponentially decreasing function, labeled by $C_{\varepsilon_i}[\xi(-a)]$ previously, which gives the wave function at $z=-a$. The R matrix at $z=-a$ and energy ε_i, is obtained from the asymptotic solution, in the form

$$R(-a,\varepsilon_i)=\frac{C_{\varepsilon_i}(\xi(-a))}{C'_{\varepsilon_i}(\xi(-a))}. \tag{44}$$

The R matrix once defined at $z=-a$, is then propagated to $z=b$, following the procedure outlined in the subsection of the strong-mixing region. At $z=b$, the asymptotic solution is defined by a combination of solutions as in Eq. (39) which, for convenience, we write in the form

$$\chi_{\varepsilon_i}(b)=S_{\varepsilon_i}(b)+C_{\varepsilon_i}(b)\tan\delta, \tag{45}$$

where δ is a phase shift; at $z=b$, we match the R matrix defined from the inside and the R matrix obtained using Eq. (45), to determine δ and thus the full continuum wave function for all z, at energy ε_i. The final continuum wave function is normalized per unit energy. Bound-state energies and eigenfunctions can also be determined using the R-matrix method [19] allowing the calculation of photoabsorption and photoionization spectra.

The method was used to determine photoabsorption and photoionization spectra in the field free case and in an electric field. Results obtained were in excellent agreement with semianalytical WKB based methods [20]. As we were especially interested in testing the accuracy of our asymptotic solutions in the photoionization case, we show in Fig. 3 the results for the photoionization spectrum of the model system for various electric fields f. As the potential is bound in the $-z$ direction, the spectra exhibit a resonance structure due to potential in $-z$. We see that the resonances have regular

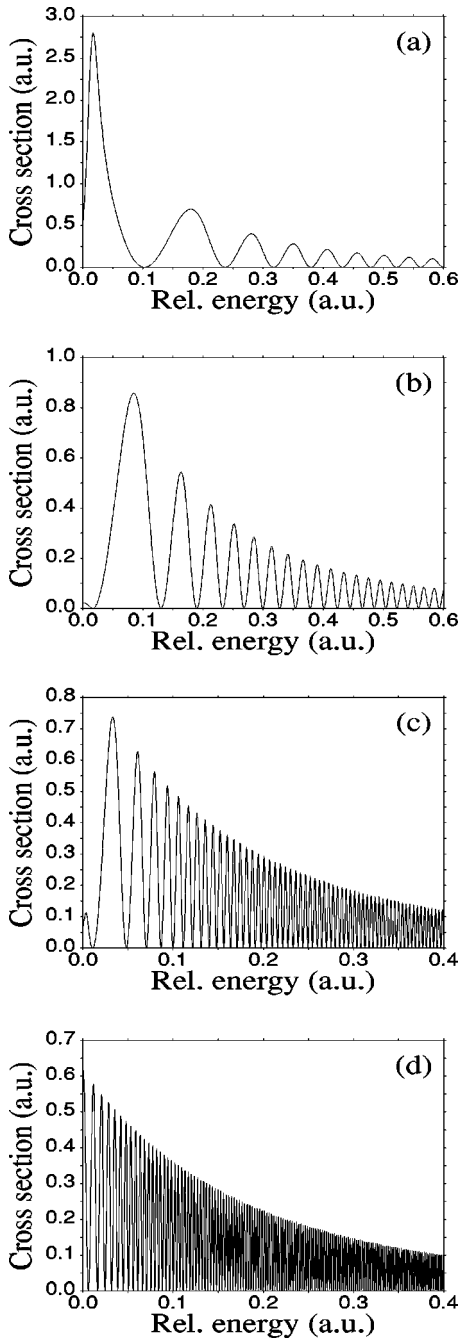

FIG. 3. Photoionization spectra for the model system in an electric field of strength f, for transitions from the ground state. The energy is relative to the classical ionization threshold and hence zero energy denotes the Stark saddle energy E_s. Four sets of spectra are produced for differing field strengths: (a) $f=1\times10^{-2}$ a.u, (b) $f=5\times10^{-3}$ a.u, (c) $f=1\times10^{-3}$ a.u., and (d) $f=5\times10^{-4}$ a.u.

spacings as is usual in Stark spectra and that the distance between resonances decreases with electric field as does their intensity. The one-dimensional nature of the potential allows for the deduction of an analytical condition using WKB giving the distance between resonances [20]. This was compared with the above numerical calculations and excellent agreement was obtained. These results show the effectiveness of our asymptotic solutions, which will be used in the main problem of an atom in parallel electric and magnetic fields.

C. The MAF asymptotic solutions in the full parallel field problem

Given that the asymptotic Hamiltonian in z for the full problem of an atom in parallel fields (28) is the same as for the one-dimensional problem, we can use the same asymptotic solutions in z in both cases. However, in the case of parallel fields, the use of the proper Coulomb term allows the integrals (36) and (37) to be solved analytically. In the proper Coulomb term, we substitute $\gamma^2(z)$ with $\Gamma^2(z)$, defined as

$$\Gamma^2(z)=2\left\{fz+\frac{1}{|z|}+\varepsilon_i\right\}. \tag{46}$$

For both of the limits $\Gamma^2(z)>0$ and $\Gamma^2(z)<0$ the expressions for $\xi(z)$ in Eqs. (36) and (37) are known in analytical form, in terms of incomplete elliptic integrals of first and second kind [21]. It can also be shown in this case that in the limit $z\rightarrow+\infty$ the above defined MAF solutions become pure Airy functions as we would expect. In fact the function $\xi(z)$ becomes

$$\xi(z)=(2f)^{1/3}\left(z+\frac{\varepsilon_i}{f}\right), \tag{47}$$

which is the argument of the Airy function solution when the Coulomb term is removed.

IV. ADIABATIC EIGENVALUE CURVES

Before describing in detail the matching between solutions at the asymptotic boundary, we describe how adiabatic solutions for the full parallel field Hamiltonian are constructed as they will be used in the matching procedure. They also give additional physical insight into the problem and may be used in certain cases to greatly simplify the numerical effort [9].

An important step in the method we developed consists in the use of R-matrix propagation technique in the strong-mixing region, which allows the evaluation of the R matrix at a distance $r=b$ from the known value at $r=a$. This however leads to an R matrix at $r=b$ containing many unwanted channels, due to the use of spherical coordinates to represent a problem that has already a symmetry very close to cylindrical. A key point is to eliminate these extra channels by calculating local adiabatic solutions. We consider an adiabatic Hamiltonian, obtained from the full Hamiltonian at a fixed radius $r=r_b$, which is given from Eq. (1), as

$$H_{ad}=\frac{L^2}{2r_b^2}-\frac{1}{r_b}+\beta L_z+\frac{1}{2}\beta^2 r_b^2\sin^2\theta-fr_b\cos\theta, \tag{48}$$

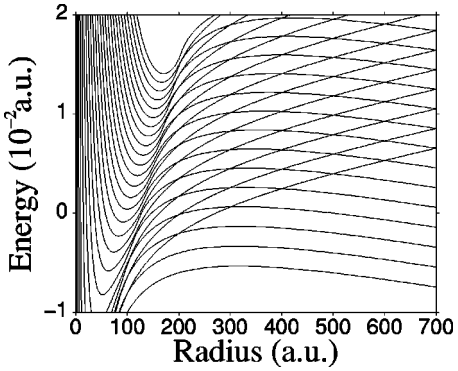

FIG. 4. Adiabatic eigenvalue curves for a hydrogen atom in parallel electric and magnetic fields of strengths 51.4 kV cm^{-1} (1×10^{-5} a.u.) and 470 T (1×10^{-3} a.u.) respectively.

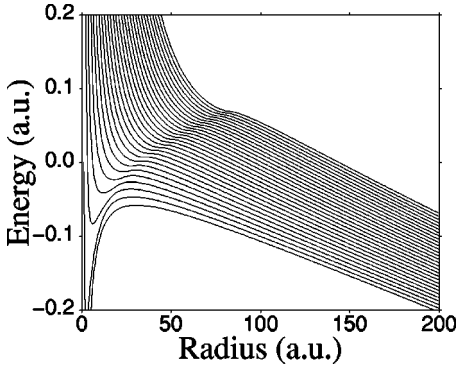

FIG. 5. Adiabatic eigenvalue curves for a hydrogen atom in parallel electric and magnetic fields of strengths 51.4 MV cm^{-1} (1×10^{-3} a.u.) and 470 T (1×10^{-3} a.u.), respectively.

where L^2 is the total angular momentum operator. This Hamiltonian has eigenvalues $\varepsilon_\lambda(r_b)$ and eigenfunctions $\phi_\lambda(r_b;\theta,\phi)$, which satisfy the adiabatic Schrödinger equation

$$H_{ad}\phi_\lambda(r_b;\theta,\phi)=\varepsilon_\lambda(r_b)\phi_\lambda(r_b;\theta,\phi). \tag{49}$$

Diagonalizing the Hamiltonian in a basis set of spherical harmonics yields a set of eigenvalues $\varepsilon_\lambda(r_b)$ and eigenvectors $c_{l\lambda}$, from which the eigenfunctions $\phi_\lambda(r_b;\theta,\varphi)$ are obtained as

$$\phi_\lambda(r_b;\theta,\phi)=\sum_l c_{l\lambda}Y_{lm}(\theta,\phi). \tag{50}$$

These functions give an exact description of the angular solutions of the Schrödinger equation at $r=r_b$ and provide a very good angular basis set in which to diagonalize the full Hamiltonian (1), when r is near $r=r_b$. In addition, this adiabatic procedure enables us to calculate the so-called adiabatic eigenvalue curves (AEC) by varying r_b in the interval $a\leqslant r\leqslant b$, and by plotting at each radius $r=r_b$, the corresponding set of eigenvalues $\varepsilon_\lambda(r_b)$. The resultant AEC are shown in Fig. 4 for electric- and magnetic-field strengths of 51.4 kV cm^{-1} and 470 T, respectively. These curves give a great deal of physical insight into the full problem, as they show how the different potentials of the system dominate at different radii.

At small radial distances from the nucleus the centrifugal barrier and then the Coulomb term dominate. Then, at increasing radial distance from the nucleus the influence of the external fields starts to become important. The splitting of the curves due to the breaking of the z symmetry by the electric field becomes obvious and shows the existence of the two different limits corresponding to $z\to-\infty$ (where the electron encounters a potential barrier) and $z\to+\infty$ (for which the electron ionizes freely at an energy above the Stark saddle energy). In a region of r between 100 and 200 a.u., avoided crossings occur and the competition between the Coulomb potential and the external fields is predominant. The Stark saddle point, obtained at a radius $r=1/\sqrt{f}\approx316$ a.u., represents the radius where the electric field begins to dominate over the Coulomb potential and the curves begin to approach straight lines.

In addition the analysis of the AEC allows the identification of two different cases, which can be understood in terms of the corresponding adiabatic angular potential at successive radii r_b [20]. Figures 4 and 5 show the different behavior of the AEC obtained for different relative values of the electric- and magnetic-field strengths. Figure 5 displays a behavior similar to the magnetic field only case and can be solved with methods developed for the case of an atom in a magnetic field only [9]. In Fig. 4, for $r<100$ a.u., the AEC are approximately the same as obtained in the magnetic field only case, because in this region of r the Coulomb field dominates. At around $r=100$ a.u. the splitting of each curve can be seen, exhibiting the breaking of symmetry with respect to the plane $z=0$, due to the presence of the electric field. One of the split lines represents a channel where the electron is moving in the $+z$ direction (with the electric field) and the other represents a channel where the electron is moving in the $-z$ direction (against the electric field). For radii larger than 400 a.u. the curves are approximately equally spaced as a consequence of the magnetic field. This spacing corresponds to the Landau energy level spacing of a particle in a magnetic field. Much of the structure observed in Figs. 4 and 5 can also be understood from the form of the angular potential from Eq. (48),

$$V_{ad}=-\frac{1}{r_b}+\beta L_z+\frac{1}{2}\beta^2 r_b^2\sin^2\theta-fr_b\cos\theta. \tag{51}$$

It can be shown that for certain combinations of field strengths and radii, ($f<\beta^2 r_b$), the two angular potentials produced by the two external fields give rise to a double potential well in θ [20]. Within each of these wells lie a series of states that correspond to the channels of the full system and have an approximate spacing of 2β. It can also be shown that if the condition for the double potential well is met, i.e., ($f<\beta^2 r_b$), then at integer multiples of β/f, the energy positions of some of the states in both wells become equal (neglecting tunneling effects). This degeneracy manifests itself in Fig. 4, where $r_b=f/\beta^2=10$ a.u., in the form of crossings as displayed in the AEC at integer multiples of

$\beta/f=100$ a.u. for those field strengths. In the case ($f \geqslant \beta^2 r_b$), because only one well exists, we do not get crossings; however, the relative increase in strength of the electric field has meant the spacing is now dependent on the electric field and matching radius and is given approximately by $\sqrt{\beta^2+f/r_b}$. Figure 5 illustrates this case and for clarity we plot the AEC up to a radius of $r=200$ a.u.

The AEC are also important to determine which channels play a role in the photoionization, for a particular energy and at a chosen matching radius. According to the AEC, channels are classified into two classes: the ones localized on the $-z$ side of the z axis, which have positive gradient, are said to be closed, and the ones localized on its $+z$ side, which have negative gradient, are said to be open. Each of these two classes of channels needs to be subdivided again, according to the total energy of the system and the particular radius considered. For a radius $r_b=b$, given an energy E, all the closed channels for which $E_\lambda<E$ are said to be locally open, and all the open channels for which $E_\lambda>E$ are said to be locally closed.

V. FRAME TRANSFORMATIONS

The general use of spherical harmonics as an angular basis set in the strong-mixing region is efficient for small values of r but becomes less efficient for larger values of r, for which the symmetry becomes predominantly cylindrical. The AEC give us guidance on how to propagate the solutions across this strong-mixing region, depending on which of the two cases ($f<\beta^2 r_b$) or ($f \geqslant \beta^2 r_b$) correspond to the field intensities of the problem. For ($f \geqslant \beta^2 r_b$), where no crossings exist, expansion and R matrix propagation in a local adiabatic basis set [9] can be very efficiently used as for the magnetic-field only problem. One uses the propagation procedure as described in Sec. II B but uses local angular eigenfunctions obtained from the diagonalization of the adiabatic Hamiltonian in each sector, instead of the spherical harmonics. This case is very similar to the magnetic-field only case and therefore will not be studied in here. However, for ($f<\beta^2 r_b$), this method is inappropriate, due to series of crossings and avoided crossings occurring, as seen in Fig. 4. In such a case we use the propagation procedure as described in Sec. II B but have the problem that the R matrix evaluated at $r=b$, from the strong-mixing region, $R_{ll'}(b)$, will contain many unwanted channels, since we are using a spherically symmetric basis set to represent the cylindrical symmetry of the Hamiltonian at $r=b$. We perform a frame transformation to a more efficient basis set, by considering the adiabatic Hamiltonian at fixed radius $r=b$, as in Sec. IV, which is diagonalized in a basis set of spherical harmonics, yielding eigenvectors $c_{\lambda l}$ and eigenvalues ε_λ. New eigenfunctions are then obtained according to Eq. (50), which provide an efficient basis set with which to represent the wave function at $r=b$ and its vicinity, as they accurately describe the angular behavior of the Hamiltonian at that radius. Hence the full wave function at the radius $r=r_b$ is written

$$\Psi(r,\theta,\phi)=\sum_\lambda \frac{F_\lambda(r)}{r}\phi_\lambda(b;\theta,\phi) \tag{52}$$

with $\phi_\lambda(b;\theta,\phi)$ as defined in Eq. (50) and $F_\lambda(r)$ the corresponding radial solution at the given radius. The R matrix expressed in terms of this new adiabatic basis set, $R_{\lambda\lambda'}$, is obtained from $R_{ll'}$, with the following frame transformation

$$R_{\lambda\lambda'}=\sum_{ll'} c_{\lambda' l'} R_{ll'} c_{l\lambda}. \tag{53}$$

The R matrix is then contracted to the number of channels of physical interest for a given energy.

VI. THE MATCHING PROCEDURE AND THE *K* MATRIX

We finally are in a position to match the solutions between the strong-mixing and asymptotic regions in order to determine the full solution over all space, and at each energy.

In the method to be followed in the matching we use the AEC corresponding to the field strengths we are treating. For each total energy, these curves will show the relation between a particular choice of matching radius and the number of channels, which should play a role in the process; this can then be checked numerically.

We exemplify the method by considering the hydrogen atom for magnetic and electric fields of intensities 51.4 kV cm^{-1} and 470 T, respectively, which correspond to the AEC given in Fig. 4.

The solutions in the asymptotic region are of the form (27) and reflect the cylindrical symmetry in the region. They are known in terms of the reactance matrix, the K matrix, which is to be determined by matching the R matrices from the asymptotic region, and the strong-mixing region, at the chosen matching radius $r=b$.

After representing the wave function in the basis set $\{\phi_\lambda(\theta,\phi)\}$, the R matrix $R_{\lambda\lambda'}$, is obtained in the form (53). It is then possible to match the R matrix in the new adiabatic basis $R_{\lambda\lambda'}$, to the asymptotic R matrix, over an arc at $r=b$, by performing a two-dimensional matching [22].

We evaluate the solutions $\{\phi_\lambda(\theta,\phi)\}$ on the arc and project them onto the asymptotic solutions (27), by integrating over θ and ϕ; this is done by evaluating the overlap integral

$$\langle \phi_\lambda | \Psi_{\varepsilon j}\rangle_{r=b}=\int \phi_\lambda \Psi_{\varepsilon j} d\Omega, \tag{54}$$

through the calculation of four matrices, $\mathbf{P},\mathbf{Q},\mathbf{P}',\mathbf{Q}'$, the elements of which are given by the following integrals

$$P_{\lambda k}(b)=\int \left[\phi_\lambda(\theta,\phi)\sum_i \Phi_i(\rho,\phi)S_{ik}(z)\right]_{r=b} d\Omega,$$

$$Q_{\lambda k}(b)=\int \left[\phi_\lambda(\theta,\phi)\sum_i \Phi_i(\rho,\phi)C_{ik}(z)\right]_{r=b} d\Omega,$$

$$P'_{\lambda k}(b)=\int\left[\phi_\lambda(\theta,\phi)\sum_i\left\{\sin\theta\frac{\partial\Phi_i}{\partial\rho}S_{ik}(z)+\cos\theta\Phi_i(\rho,\phi)\frac{dS_{ik}}{dz}\right\}\right]_{r=b}d\Omega,$$

$$Q'_{\lambda k}(b)=\int\left[\phi_\lambda(\theta,\phi)\sum_i\left\{\sin\theta\frac{\partial\Phi_i}{\partial\rho}C_{ik}(z)+\cos\theta\Phi_i(\rho,\phi)\frac{dC_{ik}}{dz}\right\}\right]_{r=b}d\Omega, \quad (55)$$

where a prime denotes differentiation with respect to the radial component r. We now have the asymptotic solutions on an arc $r=b$, and using these we can express the R matrix determined by propagation $R_{\lambda\lambda'}$, in terms of the K matrix in Eq. (27), by equating the two R matrices, as follows

$$\mathbf{R}=[\mathbf{P}+(\mathbf{QK})][\mathbf{P}'+(\mathbf{Q}'\mathbf{K})]^{-1}, \quad (56)$$

which gives the K matrix as

$$\mathbf{K}=[(\mathbf{RQ}')-\mathbf{Q}]^{-1}[(\mathbf{RP}')-\mathbf{P}]. \quad (57)$$

The K matrix must include every physically open and locally open channel with enough additional closed channels for it to be sufficiently converged. These numbers depend on the energy range under consideration and are obtained by the use of Fig. 4 as a guide, since it tells us, for any particular energy, how many open channels exist. For example, for a magnetic-field strength of 470 T and an electric-field strength of 51.4 kV cm^{-1}, there is a need to use between 1 and 4 open channels with an extra locally closed channel, in order to get sufficient convergence of the spectra over an energy range $-5.325\times10^{-3}\rightarrow0$ a.u. For simplicity, the matching radius was always chosen to be under the barrier in the $-z$ side so that the so-called closed channels are above the system's energy and we can limit ourselves to matching solutions in the $z>0$ part of the z axis; the matching of solutions in the $z<0$ part of the z axis has then no effect in the K matrix, as the asymptotic solutions there are exponentially decreasing functions and therefore give no contribution to the integrals (55).

A. Evaluation of the photoionization cross section

To evaluate the photoionization cross section we need the continuum wave function in the region where the dipole integral is nonzero. If we consider transitions from low-lying states, the corresponding wave functions are very localized about the nucleus and only the part of the continuum wave function overlapping this region will be contributing to the dipole matrix elements. This however means we must obtain the coefficients $A_{\varepsilon l}$ in Eq. (5), and in order to do that we need to discuss the renormalization of the full wave function.

1. Renormalization of the internal region wave function

As described in Sec. II B, the general derivation of the propagation-by-sector method of Stechel *et al.* [11], gives a relationship between the radial part of the wave function at $r=a$ and at $r=b$, following Eqs. (19) and (20), with the use of *global* sector R matrices. This is shown in the following expression

$$\vec{G}(a)=\mathbf{R_2}\vec{F}'(b)-\mathbf{R_1}\vec{G}'(a), \quad (58)$$

where matrices $\mathbf{R}_1$ and $\mathbf{R}_2$ are the global R matrices defined previously and determined numerically through the propagation. $\vec{G}$ and $\vec{F}$ are column vectors that contain the radial part of the total wave function at $r=a$ and $r=b$, respectively. We have defined the total wave function in the internal region by Eq. (5), where we used the set of energy-dependent constants $A_{\varepsilon l}$. But we know that $\vec{G}=\mathbf{S}\vec{A}$, where $\mathbf{S}$ is a diagonal matrix whose diagonal elements are the Coulomb functions $s_{\varepsilon l}$ and $\vec{A}$ a vector with elements $A_{\varepsilon l}$. The matrix $\mathbf{F}$ at $r=b$ is given by

$$\mathbf{F}=\mathbf{P}+\mathbf{QK}, \quad (59)$$

with $\mathbf{P}$, $\mathbf{Q}$, and $\mathbf{K}$ as defined in Eqs. (55) and (57), where $\mathbf{K}$ is now known from the matching. From Eq. (58), we obtain a set of linear equations, given by

$$(\mathbf{S}+\mathbf{R_1S}')\vec{A}=\mathbf{R_2}\vec{F}'(b), \quad (60)$$

from which we can obtain $\vec{A}$ and hence the total wave function in the internal region, via Eq. (5). The procedure for a nonhydrogenic atom would be similar with $\psi_{\varepsilon l}$ in Eq. (5) defined by Eq. (7).

2. Transformation to S-matrix normalization

Before calculating the cross section, the final stage is to renormalize the wave function so as it becomes S matrix (the scattering matrix) normalized. In this way the wave function has the correct asymptotic radial form of a superposition of an incoming and an outgoing spherical wave [12]. The transformation is simple and can be explained easily by considering the form of the radial wave functions as $r\rightarrow\infty$. From this we can express the S matrix in terms of the K matrix

$$\mathbf{S}=(\mathbf{I}+i\mathbf{K})(\mathbf{I}-i\mathbf{K})^{-1}, \quad (61)$$

where $\mathbf{I}$ is the unitary matrix; thus, to transform to S-matrix normalization we multiply the wave function by the factor

$$\mathbf{N}_S=2(\mathbf{K}-i\mathbf{I})(\mathbf{K}^2+\mathbf{I})^{-1}. \quad (62)$$

The wave function can be properly normalized now and so the photoionization cross section in parallel fields σ_P, can be evaluated for transitions from an initial bound state ψ_n to a continuum state ψ_ε. Note that ψ_ε is energy normalized since our asymptotic solutions are normalized in this way. The cross section can be expressed explicitly as

$$\sigma_P=4\alpha\pi^2\omega_{n\varepsilon}|\langle\psi_n|\mathbf{r}|\psi_\varepsilon\rangle|^2, \quad (63)$$

where $\omega_{n\varepsilon}$ is the frequency of the transition and α the fine-structure constant. The above expression for the cross section can be simplified by considering the form of the initial state

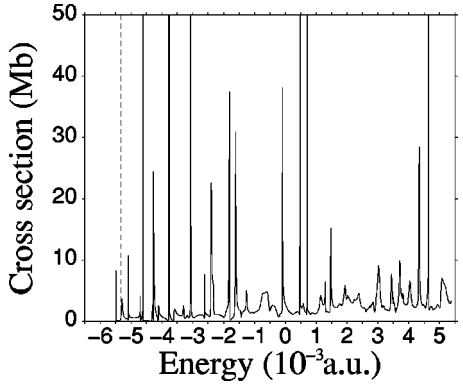

FIG. 6. The photoionization spectrum corresponding to the transition from the ground state to the $m=0$ final states of hydrogen in parallel electric and magnetic fields of field strengths $F=51.4$ kV cm^{-1} ($f=1\times10^{-5}$ a.u.) and $B=470$ T ($\beta=1\times10^{-3}$ a.u.), respectively. The dotted line represents the Stark saddle energy plus the first Landau threshold or zero-point energy.

wave function and the dipole selection rules. If, for example, we consider transitions from the ground state, then we only need to consider the form of the continuum wave function in the internal region. Also, as the ground state will be unaffected by the external fields, it can be represented by the bound state's field-free wave function. The continuum wave function within the internal region will consist of *S*-matrix normalized field free hydrogenic wave functions and hence the usual selection rules apply in order to simplify the dipole integral (63) further. In the example we are considering, the dipole selection rules dictate that only $s\rightarrow p$ transitions are allowed. Hence, only the $l=1$ partial waves of the continuum wave functions play a role and the cross section simplifies to a product of the field-free cross section and the $l=1$ components of $\vec{A}$, obtained from Eq. (60), properly *S*-matrix normalized. The cross section is then written in the form

$$\sigma_P=|A_{\varepsilon l=1}|^2\sigma_{FF}, \tag{64}$$

where $\vec{A}$ is the vector containing the renormalization coefficients of the internal region and σ_{FF} is the field-free hydrogen cross section. All the effects of the external fields on the photoionization cross section are therefore contained in $A_{\varepsilon l=1}$.

VII. ATOMIC SPECTRA

We show in Fig. 6 the photoionization spectrum evaluated for hydrogen, using the method presented here. It corresponds to transitions from the ground state to the $m=0$ final states of hydrogen in parallel electric and magnetic fields of strength 51.4 kV cm^{-1} and 470 T, respectively. The dashed line corresponds to the Stark saddle energy plus the first Landau threshold or zero-point energy, i.e., $E_0=-2\sqrt{f}+\beta$. The spectra between E_0 and the zero-field threshold contains mostly sharp well-isolated resonances, but above this level the spectra flattens as the resonances overlap and the continuum contribution increases. In Fig. 7(i) we display spectra

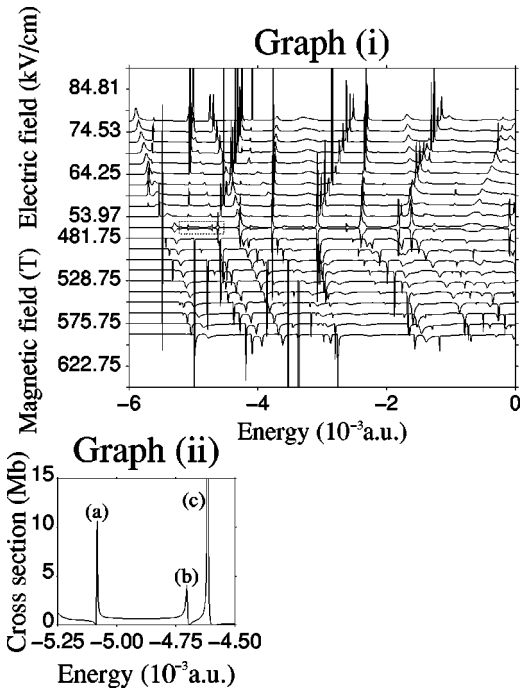

FIG. 7. Diagram (i) shows photoionization spectra corresponding to the transition from the ground state to the $m=0$ final states of hydrogen in parallel electric and magnetic fields of varying intensities. The spectrum in the center of the graph is for field strengths $F=5.14$ kV cm^{-1} ($f=1\times10^{-5}$ a.u.) and $B=470$ T ($\beta=1\times10^{-3}$ a.u.). The upper half of the graph shows spectra where the magnetic field is kept constant and the electric field is increased in increments of 2.57 kV cm^{-1} (5×10^{-7} a.u.). Similarly the lower graph represents spectra where the electric field is held constant and the magnetic field is increased in increments of 11.75 T (2.5×10^{-5} a.u.). The smaller part of the central spectrum that is enclosed by a dotted line is expanded on graph (ii) and displays the resonances that are examined in detail, with corresponding wave functions plotted in Figs. 9 and 10.

that correspond to the same atomic transition as in Fig. 6, but for varying magnetic- and electric-field strengths. This study in varying field strengths allowed us to uncover and identify three different types of resonances, labeled as (a), (b), and (c) and shown in the smaller diagram of 7(ii). The difference is seen more clearly by varying the electric field only. For type (a) resonance, the resonance energy stays approximately constant for increasing electric field, for type (b) the resonance energy increases for increasing electric field and finally for type (c) the resonance energy decreases with increasing electric field. We explain this behavior qualitatively by considering the wave functions of each different class of resonance.

A. Calculation of wave functions

The continuum wave function can be calculated using the method we described but we instead used a method devised by Buchleitner *et al.* [23], who used the complex coordinate rotation method. This served as an independent test of our method to calculate the resonance structure in the continuum. We obtained excellent agreement between the two methods for the resonance positions, as shown in Fig. 8, where we test

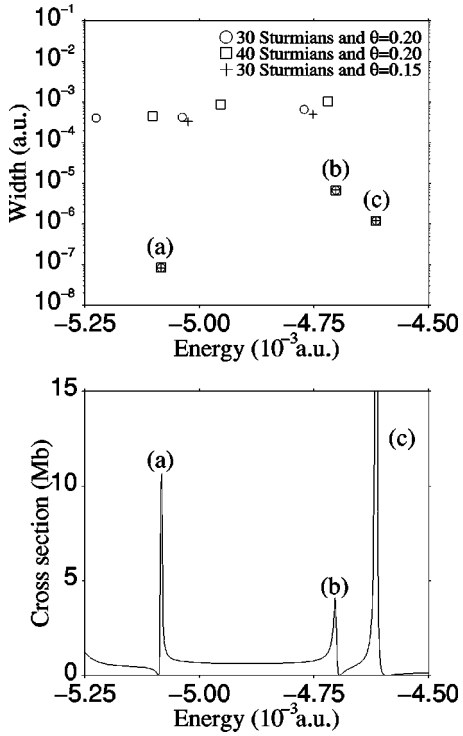

FIG. 8. Position and width of the three resonances highlighted in Fig. 7 for a hydrogen atom in parallel electric and magnetic fields of field strengths 51.4 kV cm^{-1} (1×10^{-5} a.u.) and 470 T (1×10^{-3} a.u.), respectively, as calculated by the complex coordinate method. These were calculated using a varying complex angle of rotation θ up to a value of $\theta=0.2$ rad and a Sturmian basis set of at least 30 functions. The lower figure is the same as that of diagram (ii) in Fig. 7 and it is added for comparison.

the position and width for the resonances highlighted in 7(ii). The method as described by Delande *et al.* [2] involves the diagonalization of the rotated Hamiltonian

$$H(\theta)=-\frac{e^{-2i\theta}}{2}\nabla^2-\frac{e^{-i\theta}}{r}+\beta L_z+\frac{1}{2}\beta^2\rho^2e^{2i\theta}-fze^{i\theta}, \tag{65}$$

in a basis set of Sturmian functions (radial basis set) and spherical harmonics (angular basis set). To compute resonance wave functions ([23]), applicable only to narrow resonances, one defines the approximate square of the resonance wave function as

$$|\psi_{E=\mathrm{Re}(E_{i\theta})}(\mathbf{r})|^2\approx\frac{1}{\pi|\mathrm{Im}(E_{i\theta})|}\mathrm{Re}[\psi_{i\theta}(\mathbf{r}e^{i\theta})]^2, \tag{66}$$

where $E_{i\theta}$ is the eigenvalue of the resonance, and $\psi_{i\theta}(\mathbf{r}e^{i\theta})$ is the expansion of the wave function in the Sturmian basis evaluated at a complex radius. Re and Im denote real and imaginary parts, respectively.

B. Analysis of spectra

In order to gain a physical understanding of the three types of resonances identified, labeled as (a), (b), and (c) in the diagram of Fig. 7(ii), we calculated the wave functions associated with each of them. In Fig. 9 we plot the probability densities obtained from Eq. (66) for each of the resonances (a), (b), and (c), as indicated. In Fig. 10 we show the corresponding probability densities for the resonance wave functions, on the planes $\rho=0$ and $z=0$, for clarity of analysis. Resonances of type (b) and (c) shift strongly in energy with varying applied electric fields, because their wave functions are almost entirely localized along the z axis, with only a small spread about the plane $\rho=0$. The direction of the shift can also be explained by observing that those resonances shifted in the positive energy sense have their probability densities localized mainly on the $-z$ side, as shown in Fig. 10; any such resonance will be shifted to a higher energy when increasing the electric field, as the potential barrier on the $-z$ side will be raised. The reverse argument is valid for those resonances shifted backwards, for which the increase of the electric field lowers the barrier on the $+z$ side.

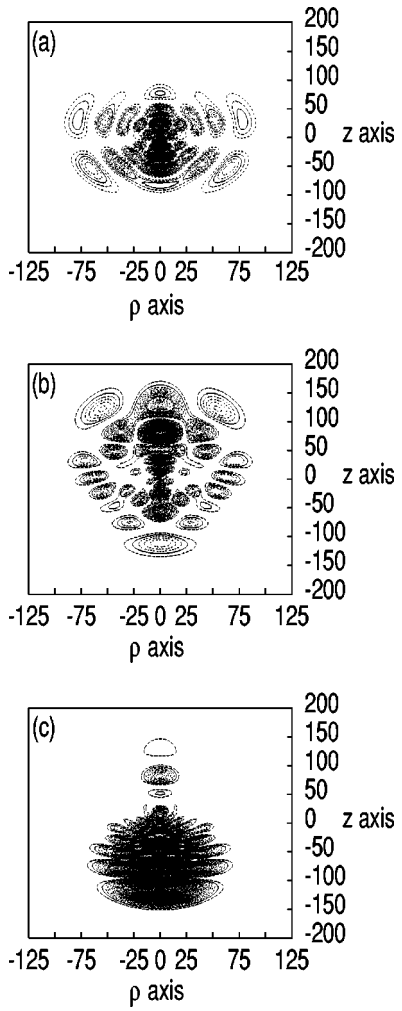

FIG. 9. Probability densities, from Eq. (66), of the resonances labelled in Fig. 7. The wave functions have been reflected about $\rho=0$ to give a clearer picture.

The resonances of type (a) which are, to a large degree, unaffected by the electric field are, as shown in Figs. 9 and 10, not entirely localized in the plane $z=0$, and have a fairly

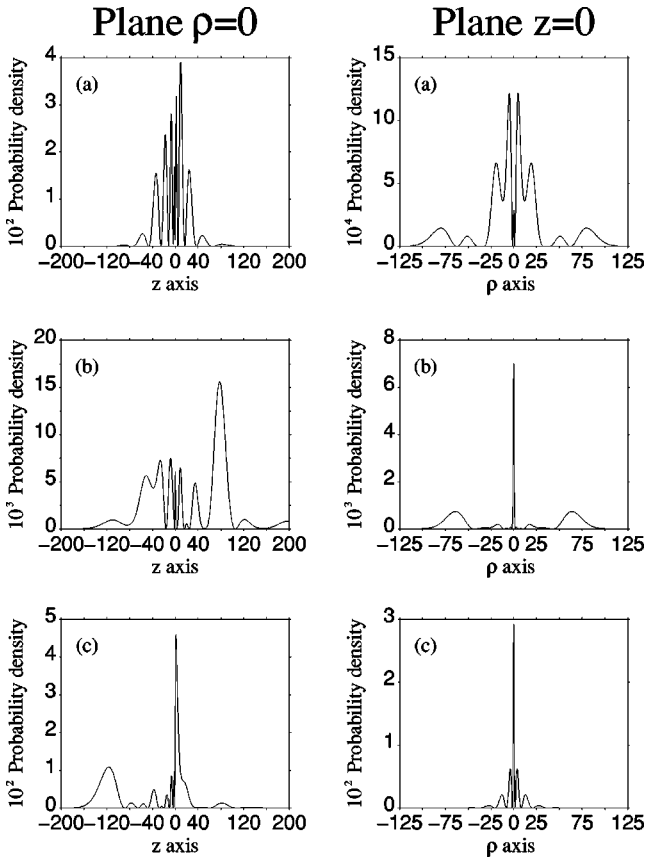

FIG. 10. Probability densities of the resonances (a), (b), and (c) labelled in Fig. 7, showing the wave functions in the respective planes $\rho=0$ and $z=0$.

large spread in ρ; their wave functions in the plane $\rho=0$ are fairly symmetric about $z=0$ and are not altered much by the electric field.

When the magnetic field is increased [lower half of Fig. 7(i)] all the resonances are shifted to a higher energy. This can be explained by the positive definite nature of the diamagnetic term, which will always increase with the magnetic field. The degree to which the shifting occurs can be explained qualitatively by the wave-function localization—resonances least affected by the electric field are the ones most shifted by the magnetic field. The reason for this behavior is due to the large spread in ρ of these resonance's wave functions, so that a change in the magnetic field has the greatest effect on them.

Other interesting features of the spectrum can be pointed out by closer inspection of the resonances of type (a), i.e., the resonances that are mostly unaffected by the electric applied field. In Fig. 11 we display three consecutive resonances of this type, enlarged from Fig. 6, which show regular spacings between them; in fact, between the first and second resonances, labeled in the figure by a_1 and a_2, respectively, we measured a spacing of $0.65\omega_c$, and between the second and the third, labeled by a_3, a value of $0.69\omega_c$ was found. This spacing suggests these resonances are connected with resonances observed in the magnetic field alone case, which occurred at regular spacings of $0.64\omega_c$ [24,25]. These resonances are quasi-Landau type resonances and are related to

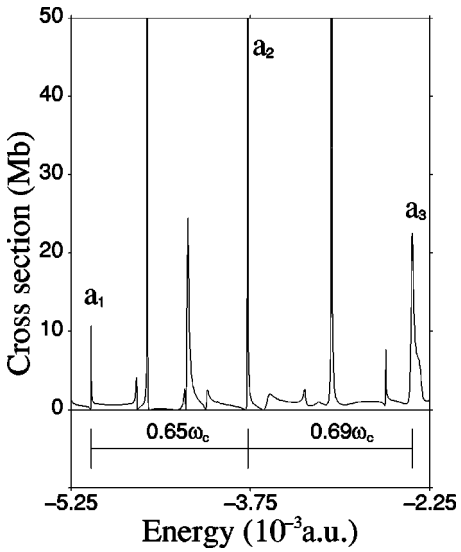

FIG. 11. The photoionization spectrum of a hydrogen atom in parallel electric and magnetic fields of strength 51.4 kV cm^{-1} (1×10^{-5} a.u.) and 470 T (1×10^{-3} a.u.). Resonances marked a_1 to a_3 are those that are mainly unaffected by increase in electric field (see Fig. 7) and we indicate the spacing between these resonances in terms of the cyclotron frequency w_c.

classical trajectories that arise from the competition between the Coulomb and magnetic fields. Observation of such resonances in the parallel field system is not surprising since, in the spectrum we considered, the magnetic field is relatively strong. The increase in spacing between the second and third resonances is caused by the modification of the orbit by the electric field. Another interesting feature related to this particular resonance is the possibility of wave function *scarring* by a periodic orbit, which means that the wave function would show a localization in the vicinity of the classical periodic orbit. This $0.64\omega_c$ orbit is known, in the magnetic-field only case, to leave the origin at an azimuthal angle of 54°; however, in the parallel field case, due to the breaking of the z parity, the angle will differ depending on which side of $z=0$ we consider. When an electric field is present, the angle in which the direction of ionization is orientated (the positive z side in our case) will increase as the orbit widens in the ρ direction to suppress ionization. In the direction opposite to the direction of ionization, the angle will decrease. For our field strengths in Fig. 11, the initial angle of the orbits trajectory in the direction of the electric field will be approximately 65°. The corresponding wave function does indeed show signs of a localization or scarring about this trajectory.

C. Spectra at laboratory strength fields

One of the great advantages of our method is that it can be applied to calculate photoionization spectra of atoms in parallel electric and magnetic fields of any strength and over extended energy regions. We show in Fig. 12 a spectrum obtained at laboratory strength fields for photoionization from the ground state of hydrogen in parallel electric and magnetic fields of strengths 0.668 kV cm^{-1} and 6.11 T, re-

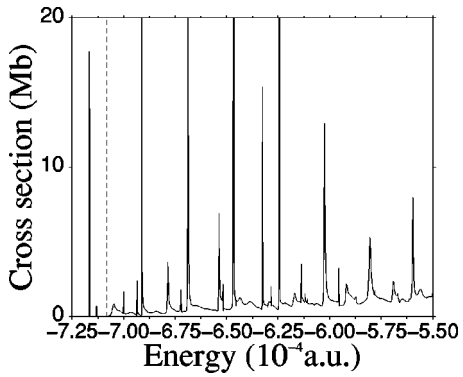

FIG. 12. The photoionization spectrum corresponding to the transition from the ground state to the $m=0$ final states of hydrogen in parallel electric and magnetic fields of field strengths 0.668 kV cm^{-1} (1.3×10^{-7} a.u.) and 6.11 T (1×10^{-5} a.u.), respectively. The dotted line represents the Stark saddle energy plus the first Landau threshold.

spectively. When considering such strength fields, we must select a greater value of matching radius b as the effect of the Coulomb potential will dominate over a larger distance. We selected a matching radius of $b=4000$ a.u. and obtained converged results.

VIII. CONCLUSION

In this paper we presented a general method to evaluate the photoionization cross section of an atom in parallel applied electric and magnetic fields of arbitrary strength. It is based on a previous method developed for an atom in a magnetic field only but takes into account the different problems faced in the parallel fields case, as for example, the breaking of the z symmetry in the associated Hamiltonian and the difficulty associated with defining the asymptotic solution due to the combination of Coulomb and electric fields. We in fact investigated three different possible forms of asymptotic solution and found that the modified Airy functions proved to be the most suitable for our purpose. We have found that the adiabatic curves for this particular problem have been very useful giving a physical understanding of the problem, and allowing us to consider two different classes of problems, depending on the relative strengths of the applied parallel fields. In the method presented here, these curves are also used as a guide to the number of channels that play a role in any given energy region and particularly at the matching radius. The adiabatic approach can also be used to generate an efficient angular basis for the R-matrix method when there are not multiple curve crossings.

We produced spectra for a hydrogen atom in parallel electric and magnetic fields for both laboratory and strong fields. In order to obtain information about the resonance structure in the spectrum, we calculated the spectra obtained for fixed electric field and varying magnetic field and for fixed magnetic field and varying electric field, around the spectrum obtained for electric and magnetic fields of 51.4 kV cm^{-1} and 470 T, respectively. We were able to identify three different types of resonance. Their behavior was explained by calculating the probability densities of the corresponding wave functions. The resonances that shifted with increasing field have a density mainly localized along the z axis and so respond to any variations of an electric field, which is orientated along the z axis; the resonances shifting in the positive energy direction have their probability distribution localized on the $-z$ side and the ones shifting in the negative energy direction have their distribution mainly on the $+z$ side. The resonances unaffected by the changing electric field have their distributions concentrated in the direction perpendicular to the z axis and are fairly symmetric about $z=0$. All the resonances were shifted to a higher energy when the magnetic field was increased, due to the positive nature of the diamagnetic term. We showed how our method works for laboratory strength fields by calculating the spectrum of hydrogen in parallel electric and magnetic fields of 0.668 kV cm^{-1} and 6.11 T, respectively.

In the future it would be of interest to systematically study the photoionization cross section and particularly the behavior of the resonance widths near the ionization threshold over a wide range of field strengths, in order to compare quantum-mechanical calculations with the behavior predicted classically by Ihra *et al.* [26].

ACKNOWLEDGMENTS

We thank Professor P. O'Mahony for useful discussions. A.S.J. was supported by EPSRC, UK. We thank the EU for financial support under their Human Capital and Mobility and Human Research Potential programs.

[1] *Irregular Atomic Systems and Quantum Chaos*, edited by J. C. Gay (Gordon and Breach Science, Switzerland, 1992).
[2] D. Delande, A. Bommier, and J.C. Gay, Phys. Rev. Lett. **66**, 141 (1991).
[3] P.F. O'Mahony and F. Mota-Furtado, Phys. Rev. Lett. **67**, 2283 (1991).
[4] S. Watanabe and H. Komine, Phys. Rev. Lett. **67**, 3227 (1991).
[5] J.P. Santos, F. Mota–Furtado, M.F. Laranjeira, and F. Parente, Phys. Rev. A **59**, 1703 (1999).
[6] I. Seipp and K.T. Taylor, J. Phys. B **27**, 2785 (1994).
[7] I. Seipp, K.T. Taylor, and W. Schweizer, J. Phys. B **29**, 1 (1996).
[8] P. Cacciani, E. Luc-Koenig, J. Pinard, C. Thomas, and S. Liberman, J. Phys. B **21**, 3473 (1988).
[9] I. Moser, Ph.D. thesis, University of London, 1997; P.F. O'Mahony, I. Moser, F. Mota-Furtado, and J.P. dos Santos in *Atoms and Molecules in Strong External Fields*, edited by P. Schmelcher and W. Schweizer (Plenum, New York, 1998), pp. 169–180.
[10] K.L. Baluja, P.G. Burke, and L.A. Morgan, Comput. Phys. Commun. **27**, 299 (1982).
[11] E.B. Stechel, R.B. Walker, and J.C. Light, J. Chem. Phys. **69**,

3518 (1978).
[12] M.J. Seaton, Rep. Prog. Phys. **46**, 167 (1983).
[13] C. Bloch, Nucl. Phys. **4**, 503 (1957).
[14] Q. Su and J.H. Eberly, Phys. Rev. A **44**, 5997 (1991).
[15] A. Rabinovitch, R. Thieberger, and M. Friedman, J. Phys. B **18**, 393 (1985).
[16] R. Thieberger, M. Friedman, and A. Rabinovitch, J. Phys. B **18**, L673 (1985).
[17] M.J. Seaton, Comput. Phys. Commun. **32**, 115 (1984).
[18] I. C. Goyal, R. L. Gallawa, and A. K. Ghatak, NIST Monograph No. 176 (National Bureau of Standards, Washington, DC, 1991); I.C. Goyal, R.L. Gallawa, and A.K. Ghatak, IEEE J. Quantum Electron. **28**, 400 (1992).
[19] M.J. Seaton, J. Phys. B **18**, 2111 (1985).
[20] A. S. Johnson, Ph.D. thesis, University of London, 2000.
[21] *Handbook of Mathematical Functions*, edited by M. Abramowitz and I. A. Stegun (Dover, New York, 1965).
[22] B. Lepetit, J.M. Launay, and M. Le Dourneuf, Chem. Phys. **106**, 103 (1986).
[23] A. Buchleitner, B. Grémaud, and D. Delande, J. Phys. B **27**, 2663 (1994).
[24] A. Holle, G. Wiebusch, J. Main, B. Hager, H. Rottke, and K.H. Welge, Phys. Rev. Lett. **56**, 2594 (1986).
[25] M.A. Al-Laithy, P.F. O'Mahony, and K.T. Taylor, J. Phys. B **19**, L773 (1986).
[26] W. Ihra, F. Mota-Furtado, and P.F. O'Mahony, Phys. Rev. A **58**, 3884 (1998).